Plasma Sources Science and Technology

Dry reforming of methane in a nanosecond repetitively pulsed discharge: Chemical kinetics modeling

To cite this article before publication: Li Zhang *et al* 2022 *Plasma Sources Sci. Technol.* in press https://doi.org/10.1088/1361-6595/ac6bbc

Dry reforming of methane in a nanosecond repetitively pulsed discharge: Chemical kinetics modeling

Li Zhang[1,2], Stijn Heijkers[2], Weizong Wang[3], Luca Matteo Martini[4], Paolo Tosi[4], Dezheng Yang[5]*, Zhi Fang[1] and Annemie Bogaerts[2]*

1 College of Electrical Engineering and Control Science, Nanjing Tech University, Nanjing, 211800, China

2 Research group PLASMANT, Department of Chemistry, University of Antwerp, Universiteitsplein 1, BE-2610 Wilrijk-Antwerp, Belgium

3 School of Astronautics, Beihang University, Beijing, 100191, China

4 Dipartimento di Fisica, Università di Trento, Italy

5 Key Lab of Materials Modification (Dalian University of Technology), Ministry of Education, Dalian, 116024, China

*Corresponding authors. E-mail addresses: annemie.bogaerts@uantwerpen.be, yangdz@dlut.edu.cn

Abstract

Nanosecond pulsed discharge plasma shows a high degree of non-equilibrium, and exhibits relatively high conversions in the dry reforming of methane. To further improve the application, a good insight of the underlying mechanisms is desired. We developed a chemical kinetics model to explore the underlying plasma chemistry in nanosecond pulsed discharge. We compared the calculated conversions and product selectivities with experimental results, and found reasonable agreement in a wide range of specific energy input. Hence, the chemical kinetics model is able to provide insight in the underlying plasma chemistry. The modelling results predict that the most important dissociation reaction of CO_2 and CH_4 is electron impact dissociation. C_2H_2 is the most abundant hydrocarbon product, and it is mainly formed upon reaction of two CH_2 radicals. Furthermore, the vibrational excitation levels of CO_2 contribute for 85% to the total dissociation of CO_2.

1. Introduction

Increasing energy demands result in high consumptions of fossil fuels, yielding serious environmental problems, such as global warming [1]. CH_4 and CO_2 are two important

greenhouse gases, causing global warming, so dry reforming of methane (DRM) is gaining increasing interest [2], to convert CO_2 and CH_4 into syngas (mixture of H_2/CO), which can further be converted into higher value chemicals and fuels by Fischer-Tropsch synthesis [3-5].

A promising technology for DRM is based on plasma, which has gained significant interest in the past decades [6-22]. Much work has been performed in a dielectric barrier discharge (DBD) [7-10], which can easily generate a stable plasma in a simple reactor design. Other discharge types are also used for DRM, such as corona discharges [11, 12], spark discharges [13-16], gliding arc (GA) discharges [17-20], microwave (MW) discharges [21, 22], atmospheric pressure glow discharges[23,24] and nanosecond pulsed discharges (NPD) [25]. Nanosecond repetitive pulses are beneficial to generate a high power density, highly energetic electrons and abundant active species [26, 27], which can significantly improve the reaction performance. Scapinello *et al.* applied an atmospheric pressure NPD for DRM, and obtained CO_2 and CH_4 conversions up to 45% and 50%, respectively [25]. The energy conversion efficiency (ECE) was reported to be about 60%, which is much larger than obtained for DBD, corona discharge and MW discharge. To further improve the application, a good insight of the underlying mechanisms is desired, which can be obtained by computer modelling of the plasma chemistry. Chemical kinetics modeling can provide information about the most important chemical reaction pathways, and has been applied for DRM in several kinds of discharges, such as GA discharge [18-20] and DBD [28-30], but to our knowledge not yet for NPDs.

Therefore, in this paper we present a chemical kinetics model to investigate the underlying plasma chemistry of DRM in NPD. For validation of the model, we compare the calculated conversion and product selectivity with experimental results. Furthermore, we explore the most important loss and formation processes of CO_2 and CH_4, as well as the most important product formation processes. Based on the insight of the main chemistry mechanisms by the chemical kinetics model, some suggestions are given to further improve the conversions or regulate the product selectivity.

2. Model description

2.1. Zero-dimensional (0D) chemical kinetics model

We used a 0D chemical kinetics model, called ZDPlasKin [31], to describe the plasma chemistry. This model calculates the species densities as a function of time by solving a set of continuity equations for all species, including the electrons, in which the time evolution of species *i* is computed using the equation:

$$\frac{d\left[N_i\right]}{dt} = \sum_{j=1}^{j_{\max}} Q_{ij}(t) \tag{1}$$

where N_i represents the number density of species *i* (in cm^{-3}), Q_{ij} represents the source rates of species *i* corresponding to different reactions *j*, and j_{max} is the total number of reactions giving rise to production of loss of that species, respectively.

The typical reactions in the plasma can be expressed as:

$$a\mathrm{A} + b\,\mathrm{B} \quad \left[+\delta\varepsilon\right] \rightarrow a'\mathrm{A} + c\mathrm{C} \quad \left[+\delta\varepsilon\right] \tag{2}$$

in which A, B and C represent the species; a, a′, b and c represent the stoichiometric coefficients of reactants or reaction products; and δ_ε represents the energy needed or released by the reaction. The reaction rate constant is expressed as:

$$R_j = k_j\left[\mathrm{A}\right]^a\left[\mathrm{B}\right]^b \tag{3}$$

where k_j is the rate constant of reaction j (in $cm^3\ s^{-1}$ or $cm^6\ s^{-1}$ for two-body or three-body reactions, respectively). So the source rates of species A, B, C corresponding to the above reaction are:

$$Q_{\mathrm{A}} = (a' - a)R,\ Q_{\mathrm{B}} = -bR,\ Q_{\mathrm{C}} = cR \tag{4}$$

2.2. Chemistry set

The chemistry set used in this study was adopted from previous models developed for DRM in DBD and GA plasma[18,32], and it includes the vibrational levels of CO_2, CO, O_2, H_2, as well as two levels for CH_4 and H_2O, besides various radicals, molecules, ions, electronic excited species and the electrons (see details in table 1 and table 2). More information about the reaction rate coefficients and the cross section can also be found in Ref. [33–49]. In the experimental results, the recoveries of both carbon, oxygen and hydrogen are total at low energy input (lower than 3 kJ dm^{-3}), and the lack of oxygen mass balance for higher energy input is mainly attributed to water formation [25], so it is

reasonable to assume that there are no oxygenated compounds in the products, or their density is low enough to be ignored. Furthermore, for DRM in other spark discharges, the hydrogen mass balance is almost 100%, only considering H_2, hydrocarbons, and H_2O [14,16,50]. Therefore, oxygenated compounds are not included in our chemistry set. About 3000 reactions are considered, including electron impact reactions, electron-ion recombination reactions, ion-ion, ion-neutral and neutral-neutral reactions, as well as vibration-translation (VT) and vibration-vibration (VV) relaxation reactions. These reactions are exactly the same as in the model of DRM by GA discharge [18], except that the reactions of the oxygenates are removed; so we refer to Ref. 18 for more information. In this model of DRM by GA discharge, the densities of oxygenated compounds were 7 or 8 orders of magnitude lower than the density of the main products (i.e., H_2 and CO).

Table 1: Species taken into account in the 0D model.*

Neutral molecules	Charged species	radicals	Excited species
CO_2, CO	CO_2^+, CO_4^+, CO^+, $C_2O_2^+$, $C_2O_3^+$, $C_2O_4^+$, C_2^+, C^+, CO_3^-, CO_4^-	C_2O, C, C_2	$CO_2(V_a, V_b, V_c, V_d)$**, CO_2 (V_1-V_{21}), $CO_2(E_1)$, CO (V_1-V_{10}), CO (E_1-E_4)
O_2, O_3	O^+, O_2^+, O_4^+, O^-, O_2^-, O_3^-, O_4^-	O	O_2 (V_1-V_4), $O_2(E_1$-$E_2)$, O(1D), O(1S)
CH_4	CH_5^+, CH_4^+, CH_3^+, CH_2^+, CH^+,	CH_3, CH_2, CH	$CH_4(V_1, V_2)$
C_2H_6, C_2H_4, C_2H_2, C_3H_8, C_3H_6	$C_2H_6^+$, $C_2H_5^+$, $C_2H_4^+$, $C_2H_3^+$, $C_2H_2^+$, C_2H^+	C_2H_5, C_2H_3, C_2H, C_3H_7, C_3H_5	
H_2	H_3^+, H_2^+, H^+, H^-	H	$H_2(V_1$-$V_{14})$, $H_2(E_1)$, H(2P)
H_2O, H_2O_2	H_3O^+, H_2O^+, OH^+, OH^-	OH, HO_2	$H_2O(V_1,V_2)$
	electrons		

* The symbols 'V' and 'E' between brackets for CO_2, CH_4, CO and O_2 represent the vibrationally and electronically excited levels of these species, respectively. The notation, energy and identification of all excited levels is given in Table 2.

** Symbols 'a-d' and '1-21' represent the effective symmetric mode levels at low energy, and the asymmetric mode vibrational levels of CO_2, respectively.

Table 2: Notation, corresponding energy and identification of the excited levels considered in the model (cf. Table 1).

	Notation	**Energy(eV)**	**Identification**
Effective symmetric vibrational mode levels of CO_2	CO_2 (V_a) CO_2 (V_b) CO_2 (V_c) CO_2 (V_d)	0.083 0.167 0.252 0.339	(0 1 0) (0 2 0) + (1 0 0) (0 3 0) + (1 1 0) (0 4 0) + (1 2 0) + (2 0 0)
Asymmetric vibrational mode levels of CO_2	CO_2 (V_1) CO_2 (V_2) CO_2 (V_3) CO_2 (V_4) CO_2 (V_5) CO_2 (V_6) CO_2 (V_7) CO_2 (V_8) CO_2 (V_9) CO_2 (V_{10}) CO_2 (V_{11}) CO_2 (V_{12}) CO_2 (V_{13}) CO_2 (V_{14}) CO_2 (V_{15}) CO_2 (V_{16}) CO_2 (V_{17}) CO_2 (V_{18}) CO_2 (V_{19}) CO_2 (V_{20}) CO_2 (V_{21})	0.29 0.58 0.86 1.14 1.43 1.70 1.97 2.24 2.51 2.77 3.03 3.29 3.55 3.80 4.04 4.29 4.53 4.77 5.01 5.24 5.47	(0 0 1) (0 0 2) (0 0 3) (0 0 4) (0 0 5) (0 0 6) (0 0 7) (0 0 8) (0 0 9) (0 0 10) (0 0 11) (0 0 12) (0 0 13) (0 0 14) (0 0 15) (0 0 16) (0 0 17) (0 0 18) (0 0 19) (0 0 20) (0 0 21)
Electronically excited level of CO_2	CO_2 (E_1)	7.0	$^1\Delta u$

Vibrational levels of CO	CO (V_1) CO (V_2) CO (V_3) CO (V_4) CO (V_5) CO (V_6) CO (V_7) CO (V_8) CO (V_9) CO (V_{10})	0.266 0.528 0.787 1.040 1.300 1.540 1.790 2.030 2.270 2.510	
Electronically excited levels of CO	CO (E_1) CO (E_2) CO (E_3) CO (E_4)	6.22 7.90 10.4 10.6	$A^3\Pi$ $A^1\Pi$ $A^3\Sigma$, $D^3\Delta$, $E^3\Sigma$, $B^3\Sigma$ $C^1\Sigma$, $E^1\Pi$, $B^1\Sigma$, $I^1\Sigma$, $D^1\Delta$
Vibrational levels of O_2	O_2 (V_1) O_2 (V_2) O_2 (V_3) O_2 (V_4)	0.19 0.38 0.57 0.75	
Vibrational levels of CH_4	CH_4 (V_1) CH_4 (V_2)	0.162 0.361	
Vibrational and electronically excited levels of H_2 and H	H_2 (V_1) H_2 (V_2) H_2 (V_3) H_2 (V_4) H_2 (V_5) H_2 (V_6) H_2 (V_7) H_2 (V_8) H_2 (V_9) H_2 (V_{10}) H_2 (V_{11}) H_2 (V_{12}) H_2 (V_{13}) H_2 (V_{14}) H_2(E_1) H(^{2}P)	0.516 1.0 1.46 1.88 2.28 2.646 2.98 3.28 3.56 3.746 4.016 4.2 4.3 4.424 8.9 10.2	 $B^3\Sigma$

2.3. 0D description of the NPD

The nanosecond pulsed discharge studied in this work is based on the experimental setup used in Ref. 25. The reactor consists of two brass disc electrodes (diameter 8 mm), placed in a quartz tube with an internal diameter of 10 mm, as shown in figure 1. The plasma is generated in a plane-to-plane configuration. The inter-electrode gap is 2.5 mm. The gas enters the reactor through holes in the top (high voltage, HV) electrode and leaves through holes in the bottom (grounded) electrode, so in the model we consider it as a plug flow reactor (see below). The input gas flow rate varies between 200 and 600 sccm, which translates in a residence time in the discharge between 36 and 12 ms, respectively. The applied voltage is a triangular pulse with a duration time of 12 ns, and a peak voltage of 15.8 kV, shown in Figure 1(b). The peak discharge current is about 180 A, measured by an I/V converter. The instantaneous (peak) power is about 2.4 MW, which is calculated as the product of voltage and current, and because there is a time delay between both of 2.15 ns. The pulse energy is the time integral of the instantaneous power, and is thus equal to about 12 mJ [25] (see also Table 3 below).

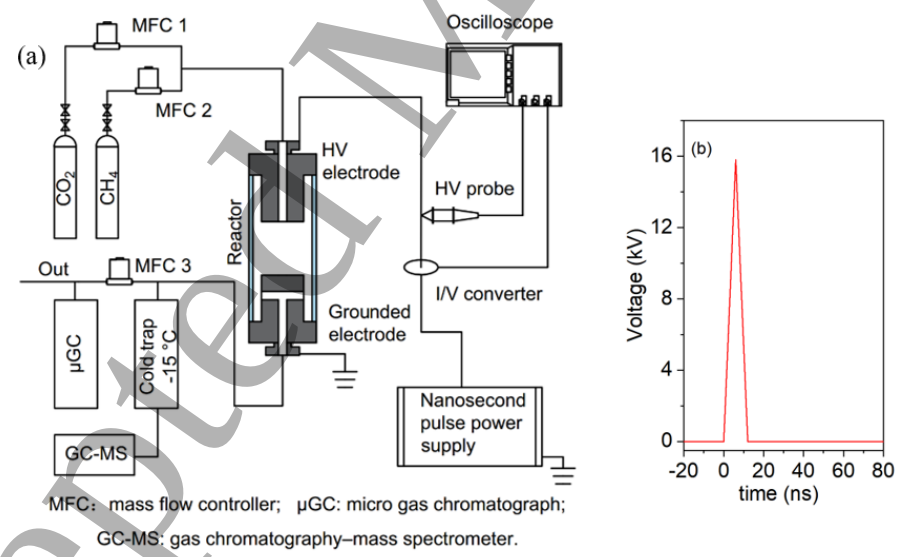

Figure 1. Schematic diagram of the experimental setup (a) and high voltage pulse (b) used in the model.

Furthermore, to model the NPD with a 0D model, we had to make some assumptions:

(1) We assume that the spark discharge channel has a length of 2.5 mm (equal to the inter-electrode gap), and a radius of 2 mm. It was observed in the experiments that these spark channels randomly appear between the electrodes, which means that electrons and other

reactive species can accumulate in the gap. Consequently, the reactions probably not only take place in the discharge channels, but also in a bit larger space. As the radius of a spark channel was reported to be 0.4 - 1.5 mm, but the radius of the gas temperature fields is a little bit larger [51,52], we use a bit larger radius (2 mm) to account for this effect. The radius of the region with high gas temperature and of the reactive species distribution area is larger than the discharge channel radius [53]. Especially the diameter of the afterglow region (which is still characterized by a high temperature and reactive species) increases compared to the radius of the spark channel. It is found that the diameter of the afterglow region increases to be larger than 3 mm after 200 μs, according to the calculations of Castela about NPD of a methane-air mixture [51]. Therefore, we use a bit larger radius (2 mm) to avoid underestimating the contribution of the reactions between the reactive species, which are determined by the higher temperature. Note that this is different from our previous model, where a constant diameter of 0.4 mm during the pulse, increasing in the afterglow, was assumed [35]. Indeed, the setup is different here (plane-to-plane configuration vs pin-to-sphere configuration in Ref. [35]). In this plane-to-plane configuration, as the discharge channels are not fixed, but appear randomly in the electrode gap, it is not possible to determine the initial gas temperature for each discharge channel, and their radius may be different for each channel, so we believe this new assumption, i.e., an average radius, is more reasonable for the setup under study here.

(2) Since the spark discharge channels appear randomly, not all molecules will pass through the discharge channels within each period of the applied voltage, which means that the time between pulses (i.e. called the afterglow in the calculations) must be longer. If we assume that the number of periods for the molecules to pass through one discharge channel is δ_{pulse}, then the afterglow time can be calculated as:

$$t_{afterglow} = t_{between} + (\delta_{pulse} - 1)(t_{pulse} + t_{between}), \quad (5)$$

where t_{pulse} and $t_{between}$ is the pulse time and the time in between two pulses. As the radius of the electrodes and discharge channels is 4 mm and 2 mm, respectively, the electrode area can contain 4 discharge channels. Considering the randomness and overlap of the discharge channels, on average the discharge can cover the whole reactor every 5-10 pulse periods. We thus assumed that each molecule experiences 1 microdischarge in 8 cycles of the applied voltage, i.e., δ_{pulse} = 8, t_{pulse} is 12 ns, and $t_{between}$ is 0.33-10 ms,

for a pulse frequency ranging from 100 Hz to 3 kHz, based on the experiments [25]. The number of discharge channels that the gas molecules can pass thorough in the residence time is $t_r/(t_{pulsed}+t_{aftergolw})$. This assumption is found to give reasonable agreement between calculation results and experiments (see below). Moreover, varying this value affects the absolute numbers of the species densities and the conversion of CO_2/CH_4 to some extent, but it was not found to change the overall picture of the important pathways (see section 3.1).

It should be noted that memory effects have been found in high frequency air DBD plasma [55]. Montesano et al investigated the discharge channel path through the ICCD images of in pure CO_2 or CO_2/CH_4 nanosecond pulsed spark discharge [56,57]. They found that the memory effects become dominant when pulse repetition frequency is higher than 10 kHz, i.e., all the subsequent discharge pulses follow the first pulse's path. But for the discharge with lower frequency (lower than 10 kHz), the discharge channel in each pulse is spatially independent. The highest pulse repetition frequency is 3 kHz in our simulation. Therefore, we didn't consider the memory effect in this model.

(3) We assume an average gas temperature of 1500 K in the model, based on reported experimental values of NPDs in methane and methane-air mixtures[51,52,58]. In principle, the gas temperature evolves over time in the discharge. However, as the discharge channels randomly appear, and it is not possible to determine the initial gas temperature of each discharge channel, it is also not possible to calculate the gas temperature evolution within each discharge channel in the 0D model. We thus assume an average gas temperature.

It is valuable to determine the gas temperature profile in future experiments with a fixed electrode configuration to get a stable discharge distribution.

The plasma is treated as a "plug flow reactor", assumed to be a radially homogeneous plasma with uniform species density and neglecting species transport in the radial direction, only considering axial transport. Although the 0D model calculates the species densities only as a function of time, it also allows following the axial variation of the plasma quantities. Indeed, it considers a volume that moves at a velocity ν calculated as:

$$v = \frac{F_m}{60A} \tag{6}$$

where F_m is the gas flow rate; $A = \pi r^2$ is the discharge channel cross-section area; and r is the discharge channel radius (2 mm).

By means of this velocity, the time dependence of the 0D chemical kinetics model can be converted into an axial dependence throughout the discharge channel. Therefore, it is possible to express the power density as a function of travelled distance $x=vt$. In the discharge process, we consider a triangular power density profile given by:

$$P_{den} = \begin{cases} \left[1 - \left|\dfrac{x-(x_{start}+L/2}{L/2}\right|\right] P_{\max}, & \text{if } x_{start} \le x \le x_{start}+L \\ 0, & \text{otherwise} \end{cases} \tag{7}$$

where L is the discharge channel length (2.5 mm); x_{start} is the axial coordinate at which the plasma starts; and P_{max} is the maximum power density (see Figure 2).

$$P_{\max} = 2 * \frac{E_{pulse}(J)}{t_{pulse}(s)AL} \tag{8}$$

where E_{pulse} is the HV pulse energy (see table 3); A is the discharge channel cross-section area; and L is the discharge channel length (2.5 mm).

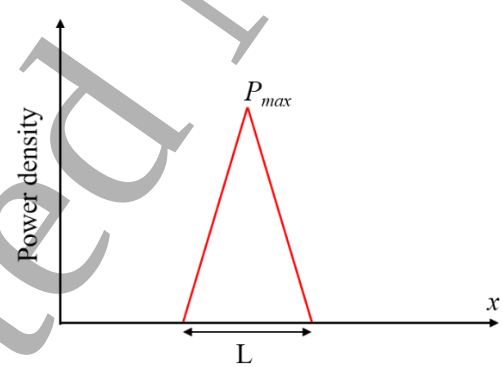

Figure 2 Power density profile considered in the model.

Although the model is 0D and only calculates the species densities as a function of time (with equation 1 in section 2.1 above), the time dependence can be translated into a spatial dependence (i.e., travelled distance of the gas through a plug flow reactor), by means of the gas flow velocity, because of the equivalence between a batch reactor and a plug flow reactor [29,32,59]. Therefore, this 0D model is also often called a quasi-1D mode [20,24,60]. The model calculates, among others, the species densities as a function of time, or position in the gap between both electrodes (travelled distance), as well as the rates of

the various chemical reactions, from which the reaction pathways for production and loss of all species can be obtained. The electron energy distribution function can also be calculated by the Boltzmann equation for electrons using the integrated Boltzmann solver (Bolsig+) in ZDPlaskin. Note that the electron energy mentioned in this paper is the average electron energy.

In addition, we also calculated the conversion and product selectivities, in a wide range of specific energy input (SEI), in order to validate the model. The SEI is defined as:

$$SEI(\text{kJ L}^{-1}) = \frac{P(\text{W}) \times 60(\text{s min}^{-1})}{\Phi_r(\text{sccm})} = \frac{f(\text{Hz}) \times E_{pulse}(\text{J}) \times 60(\text{s min}^{-1})}{\Phi_r(\text{sccm})} \tag{9}$$

where P is the power of the NPD, f is the pulse repetition frequency, ranging from 100 Hz to 3 kHz, E_{pulse} is the HV pulse energy, and Φ_r is the total gas flow rate. The SEI can thus be varied by changing the gas flow rate, the HV pulse repetition frequency or the pulse energy.

The calculated reactant conversions are defined as:

$$X_r(\%) = \left(1 - \frac{n_{r,o} v_o}{n_{r,i} v_i}\right) \times 100\%, \text{ for } r = \text{CO}_2, \text{CH}_4 \tag{10}$$

where $n_{r,o}$ and v_o are the number density (in cm^{-3}) and gas velocity (in cm s^{-1}) of reactant r at the outlet, and $n_{r,i}$ and v_i are the number density and gas velocity at the inlet, i.e., at room temperature.

The calculated product selectivity is defined as:

$$S_{H_2} = \frac{\text{n}_{\text{H}_2} v_o}{2(n_{CH_4,i} v_i - n_{CH_4,o} v_o)} \times 100\% \tag{11}$$

$$S_{CO}^{C} = \frac{\text{n}_{CO} v_o}{(n_{CH_4,i} + n_{CO_2,i}) v_i - (n_{CH_4,o} + n_{CO_2,o}) v_o} \times 100\% \tag{12}$$

$$S_{C_xH_y}^{C} = \sum_{x,y} \frac{x\, n_{C_xH_y} v_o}{(n_{CH_4,i} + n_{CO_2,i}) v_i - (n_{CH_4,o} + n_{CO_2,o}) v_o} \times 100\% \tag{13}$$

$$S^{H}_{C_xH_y} = \sum_{x,y} \frac{y\, n_{C_xH_y} v_o}{4(n_{CH_4,i} v_i - n_{CH_4,o} v_o)} \times 100\% \quad (14)$$

The superscript C or H denotes whether it is carbon-based on hydrogen-based selectivity.

3. Results and Discussion

3.1. Validation of the model

Before we use this 0D chemical kinetics model to analyze the underlying mechanisms of DRM in the NPD, we validate it against the experimental data for conversion and product selectivity. The calculated and measured conversions of CO_2 and CH_4 are plotted in figure 3 as a function of SEI, for the conditions studied in ref. 25, as listed in Table 3. The rising trends in CO_2 conversion (figure 3a) and CH_4 conversion (figure 3b) are correctly predicted by the model, and excellent quantitative agreement between calculations and experiments is reached for the CO_2 conversion, while the agreement for the CH_4 conversion is still within the experimental error bars.

Table 3: Conditions studied in the calculations and experiments. [25] *

SEI(kJ/L)	Discharge power(W)	Pulse energy (mJ)	Pulse repetition frequency (kHz)	Total gas flow rate (sccm)
2.3	18.9	12.6	1.5	500
2.9	24.4	12.2	2	500
3.5	29.2	11.7	2.5	500
3.8	38.0	12.7	3	600
4.3	35.5	11.8	3	500
5.1	33.8	11.3	3	400
6.6	32.9	11.0	3	300
8.5	28.2	11.3	2.5	200
10.0	33.2	11.1	3	200

*For all the conditions, the ratio of CO_2/CH_4 is 1/1.

Note that in the experiments, the SEI is varied up to 10 kJ/L, by varying the total gas flow rate or the repetition frequency of the nanosecond pulsed high voltage. From table 3, we can see that keeping the repetition frequency at 3 kHz, decreasing the gas flow rate from 600 to 200 sccm means that the SEI is increasing from 3.8 to 10 kJ/L, and the

conversion of both CO_2 and CH_4 increase. The reason is that the lower gas flow rate leads to a longer residence time of the gas molecules in the discharge channel. When keeping the gas flow rate constant, increasing the repetition frequency also enhances the conversion of CO_2 and CH_4. This is because increasing the repetition frequency allows the molecules to go through more discharge channels in a fixed residence time. We found that by changing the total gas flow rate or the repetition frequency, when the SEI remains constant, similar results are obtained (both of the conversion and products selectivities). Jurković et al also found that the SEI dependence of CH_4 conversion is the same for all flow rates, while there is only a little bit deviations for the CO_2 conversion (see figure 5 in Ref. [61]). These results show that the different SEI modifying methods, namely repetition frequency of voltage, plasma power and gas flow rate, do not drastically change the SEI dependence of conversion. Although in our study the SEI is changed by either changing the gas flow rate or the repetition frequency of the nanosecond pulsed voltage, comparison for the effect of SEI makes sense regardless of the method.

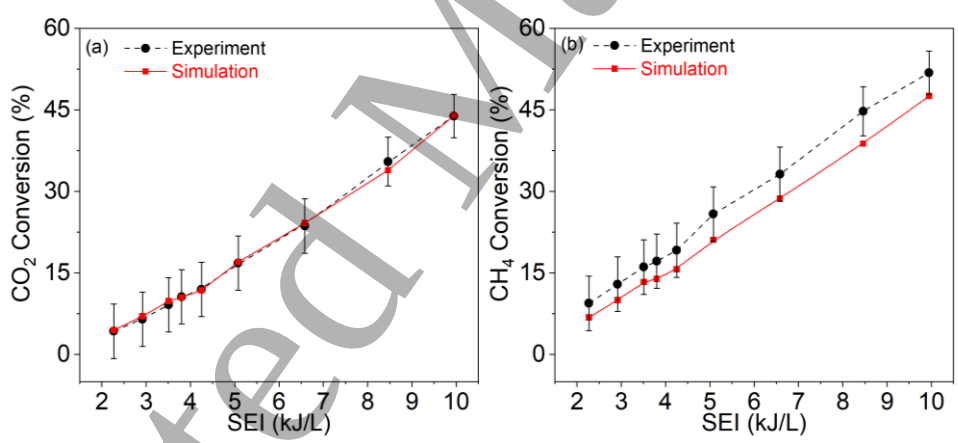

Figure 3. Measured and calculated (a) CO_2 conversion and (b) CH_4 conversion as a function of SEI.

To validate the model, we also investigated the effect of the assumption of the number of periods for the molecules to pass through one discharge channel δ_{pulse} (in assumption 2, see section 3.3). The calculated results with different δ_{pulse}, in terms of conversion and contribution of the important loss process in DRM are shown in table 4 (for SEI of 5.1 kJ/L). The results show that varying this value affects the conversion of CO_2/CH_4, but it was not found to obviously change the contributions of the important pathways, namely, no change in the order of importance of reactions (for the detailed analysis of the reaction pathways see section 3.3). As the calculated conversions using δ_{pulse} =8 show good

agreement with the experimental results, we assume that each molecule experiences 1 microdischarge in 8 cycles of the applied voltage. We realize that a 0D model is only an approximation, but a complete 3D model of the NPD, that accounts for the detailed chemistry, as well as the detailed spatial and temporal effects, would be too complex at this stage, and lead to prohibitively long calculation times. Therefore, this 0D model, despite its limitations, is considered to be acceptable, especially because it can describe the detailed chemistry within a reasonable computation time.

Table 4: Effect of δ_{pulse} on the calculated conversion and important loss process of CO_2 and CH_4.*

	Experiment	**Pulse 2**	**Pulse 4**	**Pulse 8**	**Pulse 12**	**Pulse 16**
CO_2						
Conversion	**16.81%**	63.86%	34.33%	**17.04%**	9.54%	7.03%
Dissociation process						
$CO_2 + e \rightarrow CO + O + e$		55.1%	55.6%	**56.3%**	57.1%	58.1%
$CO_2 + H \rightarrow CO + OH$		34.9%	34.1%	**32.7%**	30.7%	29%
$CO_2 + M \rightarrow CO + O + M$		10%	10.3%	**11%**	12.2%	13%
CH_4						
Conversion	**25.83%**	59.71%	36.78%	**21.76%**	13.06%	10.06%
Dissociation process						
$CH_4 + e \rightarrow CH_3 + H + e$		36.6%	35.9%	**35%**	34.8%	34.3%
$CH_4 + H \rightarrow CH_3 + H_2$		17.5%	17.2%	**16.8%**	16.4%	16.2%
$CH_4 + OH \rightarrow CH_3 + H_2O$		14%	14.6%	**15.5%**	15.7%	16.1%
$CH_4 + O \rightarrow CH_3 + OH$		16.9%	16.4%	**16%**	15.8%	15.8%
$CH_4 + C_2H_5 \rightarrow CH_3 + C_2H_6$		4%	4.8%	**5.6%**	5.8%	5.9%
$CH_4 + M \rightarrow CH_3 + H + M$		3.8%	4.1%	**4%**	4.3%	4.7%

* The SEI is 5.1 kJ/L

The calculated and measured (C-based and H-based) selectivities of the products are plotted against SEI values in figure 4. The calculated CO and H_2 selectivities are more or less consistent with the experimental result within the experimental error. Furthermore, the decreasing trends of the hydrocarbon selectivity upon increasing SEI are also reproduced in the model. In general, we consider the agreement between calculated and measured

selectivities as fairly good, in view of the complex chemistry and the approximations that we had to make in the 0D model to describe the NPD.

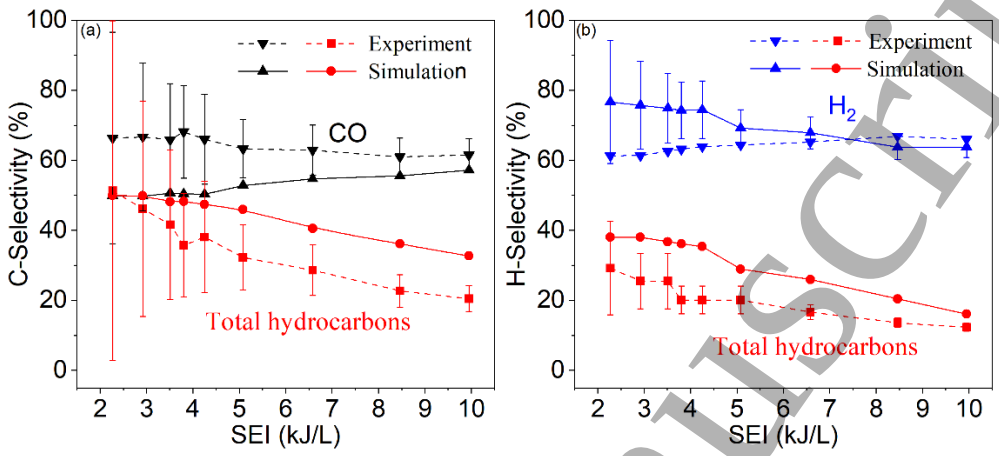

Figure 4. Measured and calculated product selectivity of (a) CO and hydrocarbons (with respect to carbon), and (b) H_2 and hydrocarbons (with respect to hydrogen).

3.2 Calculated species densities in the NPD plasma

Figure 5 shows the time evolution of the most important species densities, during the first pulse (12 ns) and afterglow ($t_{afterglow}$ = 2.7 ms, at the pulse frequency of 3 kHz investigated here). We consider a 1/1 ratio of CO_2/CH_4, and the SEI is 5.1 kJ/L. Figure 5(a, b) illustrates the stable molecules produced from DRM, in which the hydrocarbons are generated in the afterglow, much later than CO and H_2. In contrast, the densities of the radicals, ions and electrons, depicted in figure 5(c, d), also vary significantly during the pulse, but drop to negligible values after the pulse. Compared with the ions, the radicals have higher densities (typically more than an order of magnitude) and a considerably longer lifetime in the afterglow.

From the densities of the syngas components, CO and H_2 (depicted in figure 5(a)), we can deduce that the H_2/CO ratio during and shortly after the pulse is about 0.5. However, after about 600 ns, the CO density stays almost constant, while the H_2 density continues to increase, and at the end of the afterglow, before the next pulse starts, the H_2 density becomes slightly higher than the CO density. This is because most of the CO molecules are formed by electron impact dissociation of CO_2 (contribution of 56% here, see section 3.3.1) during the pulse (which is characterized by a high electron density, in the order of 10^{15} cm^{-3} at the conditions under study here; see figure 4(d)), while the most important

production of H_2 is the reaction between CH_4 and H radicals and the dissociation reaction of C_2H_4 (contribution of 60% and 21%, respectively, see section 3.3.1), in which the latter reaction mainly occurs in the afterglow.

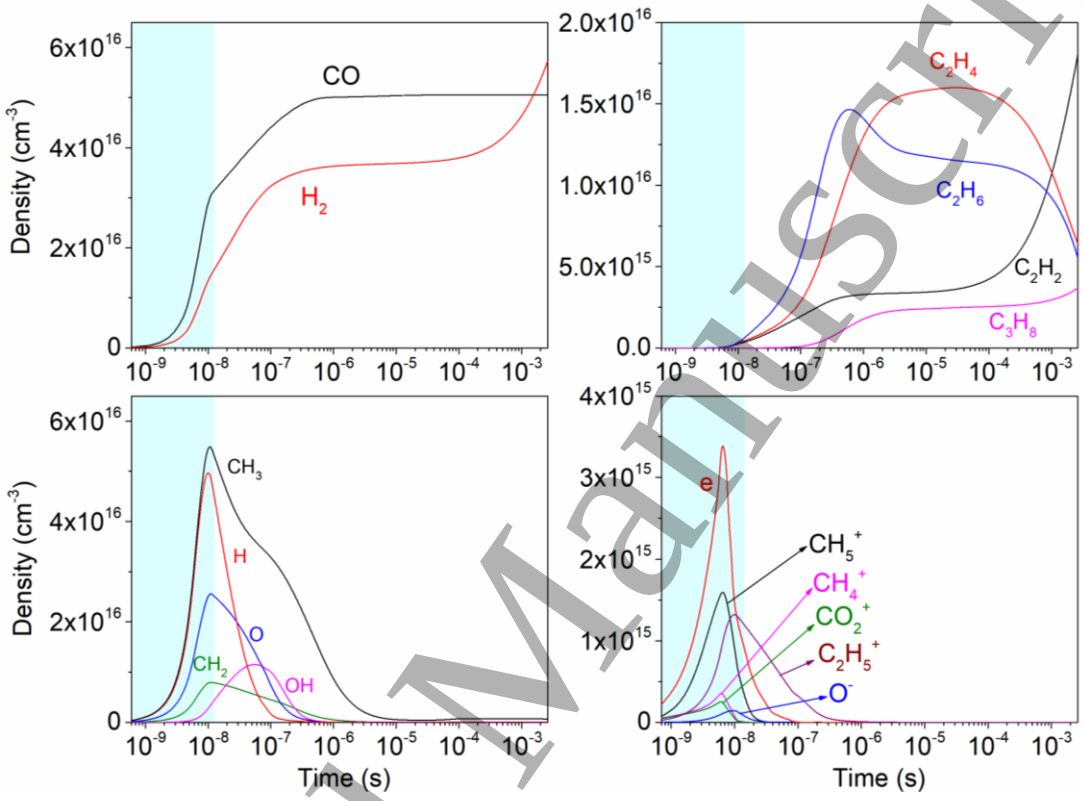

Figure 5. Calculated densities of the most important species formed in the plasma, i.e., CO and H_2 molecules (a), hydrocarbons (b), radicals (c), ions and electrons (d), as a function of time during one pulse (12 ns) and afterglow (i.e., 2.7 ms at the pulse frequency of 3 kHz studied here). The SEI is 5.1 kJ/L. The cyan region in the figure indicates the pulse time (12 ns). Note that in order to show the densities clearly, the density scales in the figures are different.

For the densities of the hydrocarbon molecules, i.e., C_2H_6, C_2H_4, C_2H_2, and C_3H_8, plotted in figure 5(b), we can see that C_3H_8 is formed later than the C_2 hydrocarbons, because it is created by reactions between C_2 hydrocarbons and radicals (or H_2, CH_4, see section 3.3.2). The densities of C_2H_6 and C_2H_4 decrease in the afterglow, whereas the densities of C_3H_8 and especially C_2H_2 continue to grow. After 1 ms, the density of C_2H_2 is higher than for the other hydrocarbons, i.e., C_2H_2 is predicted to be the most abundant hydrocarbon product in the NPD, similar to a GA discharge or spark discharge [7,16,18], while in a DBD, C_2H_6 is the dominant hydrocarbon product [10].

From figure 5(c) we can see that CH_3 and H are the most important radicals, as they are formed directly upon electron impact dissociation of CH_4. Note that the CH_3 and H densities are even higher than the molecule densities during the pulse, but they recombine into stable molecules immediately after the pulse. The lifetime of these radicals is about 0.15 - 3 μs.

The positive ions (e.g., CH_5^+, CH_4^+, and CO_2^+) and electrons are only present during the pulse (see figure 5(d)), as they recombine immediately after the pulse, and thus become negligible when there is no power deposition anymore. O^- is also formed during the pulse, but a bit later than the positive ions. The densities of the ions are, however, one order of magnitude lower than the densities of molecules and radicals in the plasma.

3.3. Underlying plasma chemistry of DRM in the NPD

As the agreement between calculated and measured conversions and product selectivities is quite good, in a wide range of SEI values, our chemical kinetics model can most probably provide a realistic picture of the plasma chemistry of DRM in the NPD. Therefore, we can now explore the underlying plasma chemistry in more detail, i.e., the loss and formation processes of CO_2 and CH_4, and the formation of the important products, as predicted by the model, and we do this again for a 1/1 ratio of CO_2/CH_4.

3.3.1 Loss and formation processes of CO_2 and CH_4

Figure 6 illustrates the time-integrated rates and the relative contributions of the major loss and formation processes of CO_2, as a function of SEI. As is clear from figure 6(a, c), electron impact dissociation of CO_2 into CO and O is the dominant loss process, with a relative contribution around 54-60% in the entire SEI range. This is different from DRM in DBD and GA, where the reaction of CO_2 with H atoms, yielding CO and OH is most important [18,30]. This reaction is also the second most important loss channel of CO_2 in our case, with a relative contribution of 25-40%, slightly rising upon higher SEI values. The dissociation reaction upon collision with any molecule M only has a minor contribution of about 5-14%, slightly decreasing upon higher SEI values. Note that we take here the sum of the dissociation reactions from the ground state and vibrational levels of CO_2, but the relative contribution of the different levels to CO_2 loss will be discussed in section 3.4.

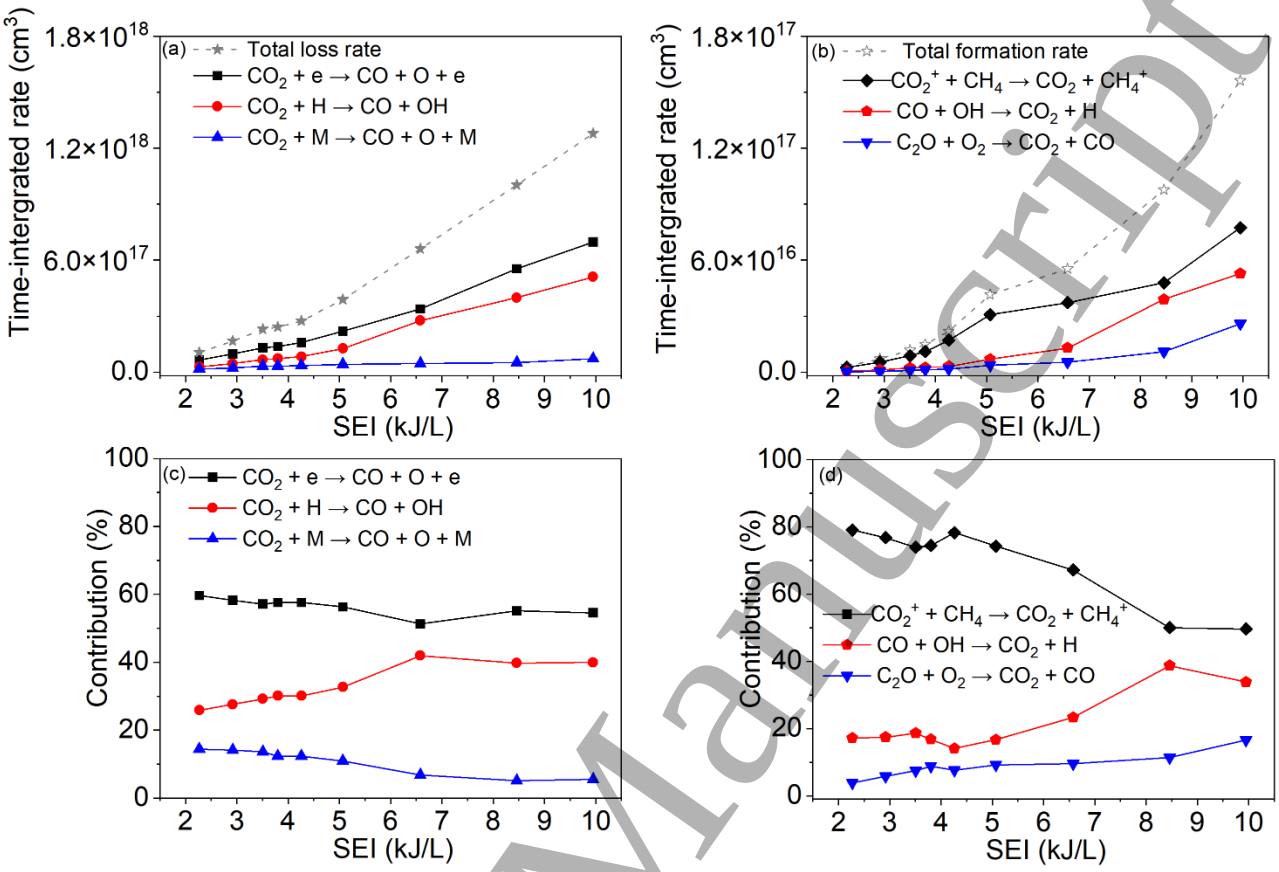

Figure 6. Time-integrated rates (a, b) and relative contributions (c, d) of the most important loss (a, c) and formation (b, d) processes of CO_2, as a function of SEI. The total time-integrated loss and formation rates are also indicated in (a, b), in grey dashed lines.

As shown in figure 6(b, d), the charge transfer reaction of CH_4 with CO_2^+ is the most significant formation process of CO_2, with a relative contribution around 45-80%, decreasing upon higher SEI. The reaction between CO and OH radicals becomes gradually more important with increasing SEI (from 20% to 40%), while the reaction of C_2O with O_2 has a minor contribution (up to 10%) to the production of CO_2.

When comparing the rates of the loss and formation reactions (figure 6(a, b)), it is clear that CO_2 formation is one order of magnitude less important than CO_2 loss. In other words, the rates of the reverse reactions (e.g., reaction of CH_4 with CO_2^+, and recombination of CO with OH radicals into CO_2 and H) are less than 10% of the forward reaction rates (loss of CO_2).

If we take a look at the CH_4 loss processes, the most important reaction is again electron impact dissociation of CH_4 into CH_3 and H, as shown in figure 7(a, c), with a relative

contribution of 25-40%, rising with SEI. This is also different from DRM in a GA, where the reaction of CH_4 with OH radicals is the dominant CH_4 loss process [18]. This reaction is also important in the NPD, as well as the reaction with H or O atoms, which contribute each for about 10-20% to the CH_4 dissociation, in the entire SEI range. Finally, C_2H_5 radicals and other molecules M also contribute to CH_4 dissociation, but their contributions are less than 10%. Bouwman et al. [62] recently presented new cross sections for electron impact dissociation of CH_4 into CH_3 and H, and reported that the values for electron energies in the range of 10-30 eV are higher than other published data sets. However, the average electron energy is around 4-7 eV in all our calculated conditions, and the maximum electron energy for the highest SEI (10 kJ/L) is about 8.6 eV. So it should not affect our results.

It is thus clear that the electrons play a more important role in the NPD than in GA plasma, for both CO_2 and CH_4 dissociation, because a lot of electrons are created during the short intense pulses, and with high enough energy to cause electron impact dissociation. Indeed, the reduced electric field in the NPD is above 200 Td insides the pulses, while it is only 50-100 Td in GA plasma [18]. This yields an electron energy around 4-7 eV (compared to 1-2 eV in GA plasma), which is high enough for direct electron impact dissociation of the CH_4 and CO_2 molecules (typically through electronic dissociative excitation from both ground and vibrational states, see table 4 in sec.3.4).

Figure 7(b, d) shows that three-body recombination of CH_3 and H is the dominant formation process of CH_4, with a contribution of 45-60%. This three-body recombination reaction is an exothermic reaction, which means that it can give rise to gas heating. On the other hand, the gas heating in NPD can also be attributed to VT relaxation of CO_2, as 80% of CO_2 is populated into vibrational states during the pulse duration (see section 3.4). However, as the discharge channels randomly appear in this NPD configuration, it is not possible to determine the initial gas temperature for each discharge channel and to calculate the evolution of the gas temperature. In our previous work about NPD of CO_2, it is found that three-body recombination of CO and O, as well as VT relaxation, which transfers energy from the CO_2 vibrational levels into translational modes of freedom, both contribute on average with 35% to the overall gas heating [54]. Other recombination reactions of CH_3,

i.e., with C_2H_6, C_2H_5, and H_2, also contribute to the formation of CH_4, for about 20-30%, 15%, and 5%, respectively. They can also give rise to gas heating.

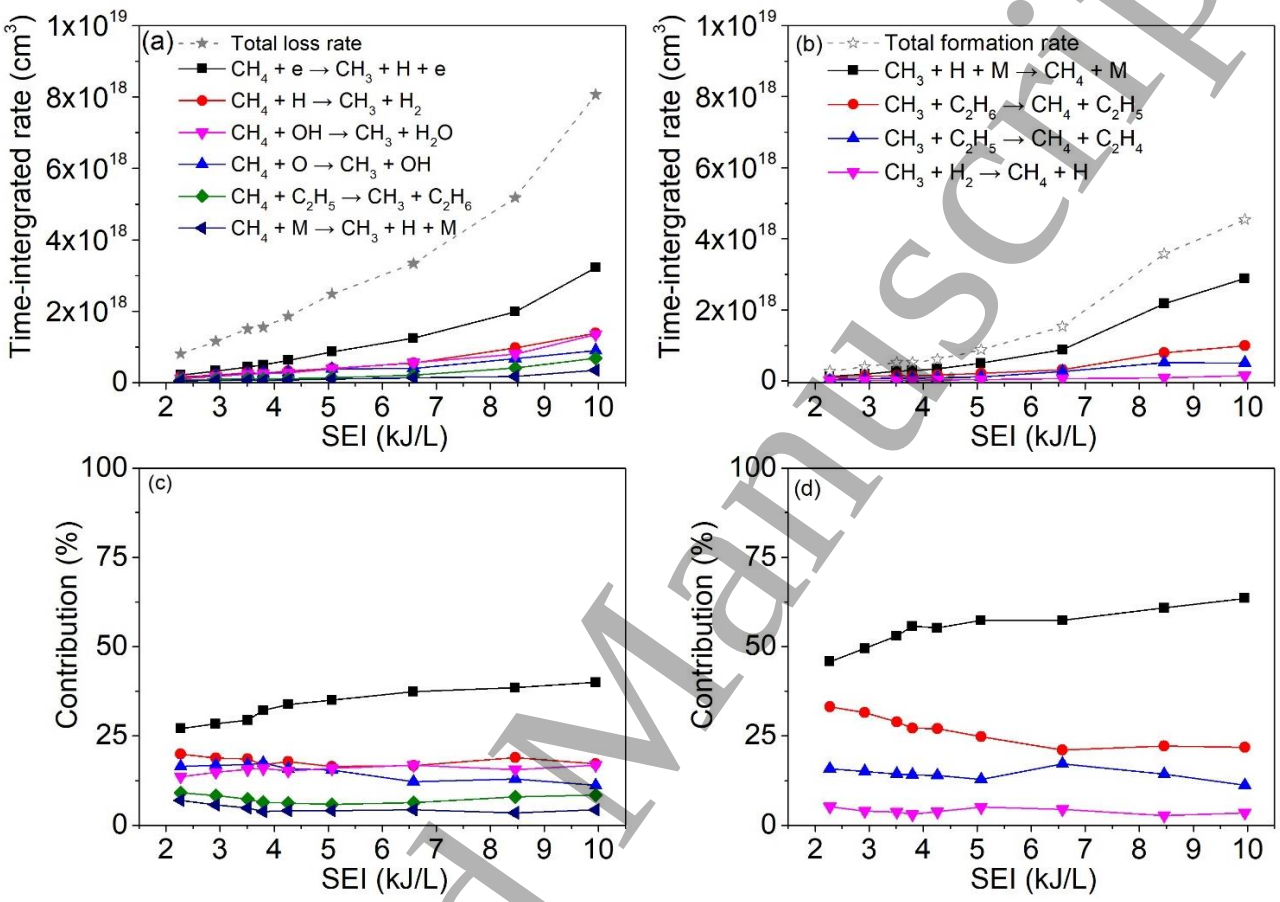

Figure 7. Time-integrated rates (a, b) and relative contributions (c, d) of the most important loss (a, c) and formation (b, d) processes of CH_4, as a function of SEI. The total time-integrated loss and formation rates are also indicated in (a, b), in grey dashed lines.

It is important to note that the total formation rate of CH_4 is only about 50% lower than the total loss rate (see figure 7(a, b)). This means that a significant fraction of the CH_3 radicals produced upon (mainly electron impact) dissociation of CH_4 during the pulses, will recombine again with H atoms (and other radicals/molecules) into CH_4 in between two pulses. This is different from the dissociation of CO_2, where the formation rate was only about 10% of the loss rate (see figure 6(a, b) above).

In other words, when comparing figure 6(a) with figure 7(a), we can see that the total loss rate of CH_4 is almost an order of magnitude higher than the total loss rate of CO_2, which is explained by the lower C-H bond dissociation energy compared to the C=O double

bond dissociation energy, facilitating electron impact dissociation, but because the formation rate of CH_4 is only 50% lower than the loss rate, the net dissociation rate of CH_4 is comparable to the net dissociation rate of CO_2, as evidenced by the similar conversions, plotted in figure 3. A similar behavior was reported for DRM in DBD plasmas, where the absolute CH_4 dissociation was higher but occurred mainly during the pulses (i.e., micro-discharge filaments), and recombination took place in between the pulses, while the CO_2 dissociation rate was lower, but occurred both during and in between the pulses [29].

3.3.2 Formation processes of the important products

As the main product of DRM is syngas (CO and H_2), we present in figure 8 the relative contributions of the major formation processes of H_2 and CO. Electron impact dissociation of CO_2 is the dominant formation process of CO, with a nearly constant contribution of 50% over the entire SEI range investigated. It is followed by the reaction between CO_2 and H radicals, which contributes for 20-30%, rising with SEI. In addition, some other reactions also contribute to CO formation, but with relative contributions below 10%.

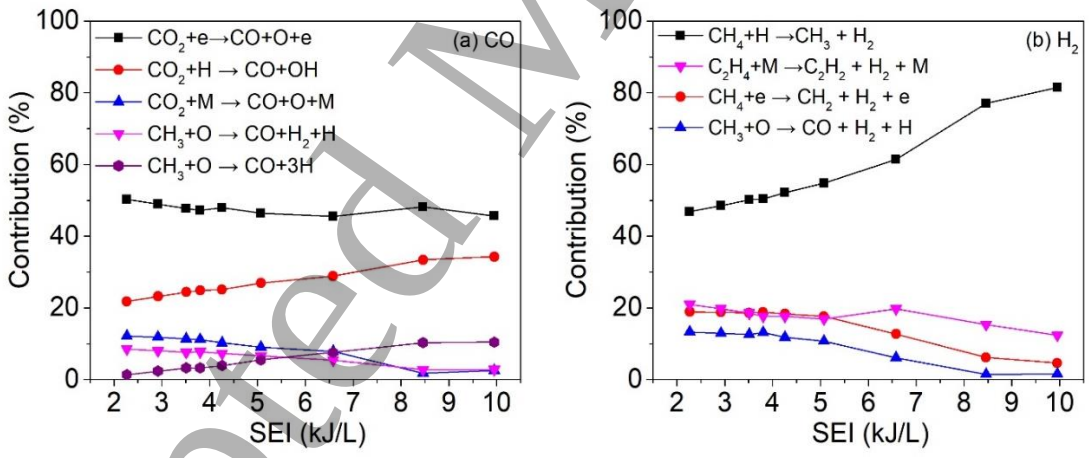

Figure 8. Relative contributions of the most important formation processes of CO (a) and H_2 (b) as a function of SEI.

It is clear from figure 8(b) that the most important production process of H_2 is the reaction of CH_4 with H radicals (contribution of 50 - 80%, clearly rising with increasing SEI), producing H_2 and CH_3 radicals. Furthermore, dissociation of C_2H_4 upon collision with any molecule M is also an important formation process of H_2, contributing for 20% in the entire SEI range. Another electron impact dissociation process of CH_4 into CH_2 and H_2 also contributes for about 10 - 20% to H_2 formation, decreasing upon higher SEI. Finally, the

reaction of CH_3 with O atoms contributes for 15% to H_2 formation at low SEI (lower than 5.1 kJ/L), but it becomes of minor importance at high SEI values.

The light hydrocarbons are also significant products of DRM in the NPD. The relative contributions of the most important formation processes of these hydrocarbons are plotted in figure 9. The dominant formation process of C_2H_2 is the reaction between two CH_2 radicals, as well as the reaction of C_2H_4 with any molecules M (contributing for 30-45% and 15-39%, decreasing upon higher SEI; see figure 9(a)). The reaction between $C_2H_3^+$ ions and H_2O is also quite important, especially at high SEI (where it contributes up to 23%). Besides, electron impact dissociation of C_3H_6, and reaction of C_3H_5 with any molecules M also contribute (for 3-10% and 4-15%, respectively) to the formation of C_2H_2.

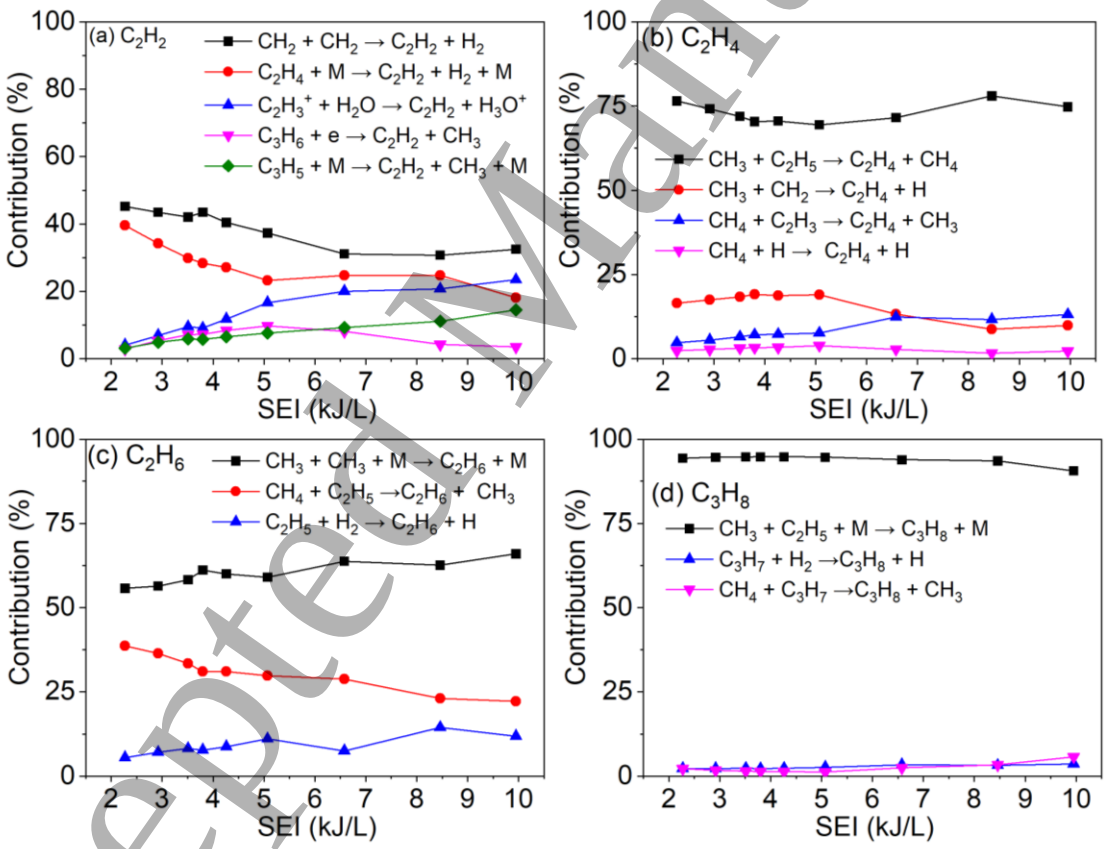

Figure 9. Relative contribution of the most important formation processes of the hydrocarbons, i.e., C_2H_2 (a), C_2H_4 (b), C_2H_6 (c), and C_3H_8 (d), as a function of SEI.

By far the most important formation reaction of C_2H_4 is the reaction of CH_3 and C_2H_5 radicals, with a contribution of about 75% in the entire SEI range; see figure 9(b). Other

formation processes are the recombination of CH_3 and CH_2 radicals, as well as the reactions of CH_4 with C_2H_3 or H, but they contribute for less than 20%.

Figure 9(c) shows that the three-body recombination of two CH_3 radicals is the most important formation process of C_2H_6, with a contribution of 55-65%. The reaction of CH_4 with C_2H_5 also plays an important role, contributing for 22-38%, decreasing upon rising SEI, while the reaction of C_2H_5 with H_2 is of minor importance.

Finally, the dominant formation channel for C_3H_8 is three-body recombination of CH_3 and C_2H_5 radicals, which contributes for more than 90% (see figure 9(d)). Other formation reactions, i.e., reactions of C_3H_7 with H_2 or CH_4 only contribute for a few % to the formation of C_3H_8.

3.3.3 Overall reaction pathways for the conversion of CH_4 and CO_2 into the major products

Figure 10 presents an overview of the dominant reaction pathways of CO_2 and CH_4 conversion into the major products (including CO, H_2, higher hydrocarbons and water). The thickness of the arrow lines corresponds to the relative importance of the net reactions (i.e., forward minus back reaction). We can conclude that CH_4 is dissociated into CH_3 and CH_2 radicals (by electron impact reaction and reaction with H, OH or O radicals), which can recombine into higher hydrocarbons (i.e., C_2H_2, C_2H_4, C_2H_6, C_3H_8). The dissociation of CH_4 and of these hydrocarbons also produces H_2. The dissociation of CO_2, mainly caused by electron impact reaction and reaction with H atoms, forms CO and O, and the O atoms react further into water via an intermediate step of OH radicals (formed upon reaction of O atoms with CH_4 and its dissociations product, i.e., CH_3 radicals).

When we compare this figure with the reaction pathways for DRM in a DBD (cf. figure 11 in Ref. [63]), it is clear that the dehydrogenation process of CH_4 in a NPD is much more prominent than in a DBD, i.e., CH_4 is mainly dissociated into CH_3 radicals (recombining mostly into C_2H_6) in a DBD, while CH_4 can be directly dissociated into CH_3, CH_2 and CH radicals by electron impact reaction in a NPD. Furthermore, C atoms can also be directly formed by electron impact dissociation of CH_4 (note however that the production rate of C atoms is three orders of magnitude lower than the CH_3 production rate, so it is indicated by a thin grey line in figure 10). This is because the NPD has a higher electron density and electron energy, i.e., in our case, the electron density and energy are about 10^{15} cm^{-3} and 4

- 7 eV (depending on the SEI), respectively, while the electron density and energy in a DBD are about 10^{13} cm^{-3} and 3 eV, respectively [29]. Hence, the density of CH_2 radicals is much higher than in a DBD, so that C_2H_2 becomes the most abundant hydrocarbon product in the NPD, because the recombination reaction of two CH_2 radicals is the most important production process of C_2H_2, as shown in figure 9(a). Moreover, the higher temperature in the NPD, causing the dissociation of the higher hydrocarbons (i.e., C_2H_4 and C_3H_5) upon collision with any molecules M (see figure 9(a)), also enhanced the formation of C_2H_2.

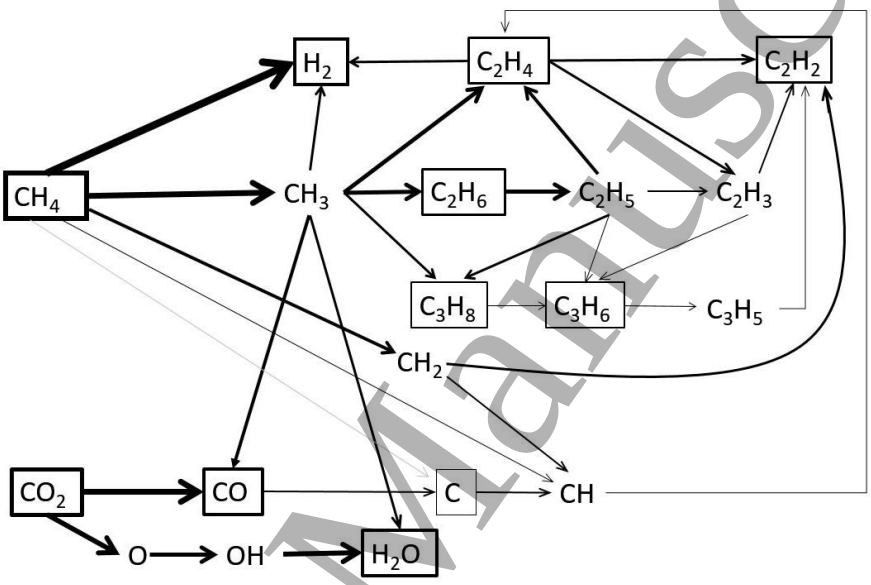

Figure 10. The dominant reactions pathways of DRM in the NPD for a SEI of 5.1 kJ/L. The ratio of CH_4/CO_2 is 1/1. The thickness of the arrow lines indicates the importance of the reaction path.

Compared with the reaction pathways in a GA discharge[18], where reactions with radicals (OH, H, O) are most prominent, the main loss processes of both CH_4 and CO_2 in the NPD are electron impact dissociation. This is again because the reduced electric field in the NPD is much higher than in a GA plasma, resulting in a higher electron energy in the NPD. It should be pointed out that, although C_2H_2 has the highest concentration of the hydrocarbon products both in NPD and GA discharge, its production processes are different. The recombination reaction of two CH_2 radicals is the most important production process of C_2H_2 in the NPD, while the most important production process of C_2H_2 in a GA discharge is the dissociation of higher hydrocarbons, which is the second important production process in the NPD. The difference is attributed to the fact that the GA plasma has a very high gas temperature (i.e., around 3500 K in the arc colume, and ca. 2700 K in the thermal area around it) [18], while we assume an average gas temperature of 1500 K

for the NPD in our model, based on experiments for methane and methane/air mixtures (see section 2.3 above).

Oxygenated compounds are not included in our chemistry set, but it does not affect our model to describe the underlying plasma chemistry of DRM in the NPD, as oxygenated compounds were also not detected in the experiments [25]. Furthermore, also according to the model for the GA discharge, where these oxygenated compounds were included, their densities were 7 or 8 orders of magnitude lower than the density of the main products (i.e., H_2 and CO) in DRM in the GA discharge [18].

3.4. Role of the CO_2 vibrational levels in DRM by the NPD

As presented in section 2, we have taken into account several vibrational levels in our model, with most emphasis to the CO_2 vibrational levels, as they play an important role in CO_2 dissociation in various types of plasmas, such as MW [63–66] and GA plasmas [67–72], as well as in NPD in pure CO_2 [54]. Figure 11 shows the vibrational distribution function (VDF) of CO_2 in the NPD at five different times, i.e., at 0 ns (the initial time, where the CO_2 vibrational population is calculated according to a Boltzmann distribution at the plasma gas temperature, i.e., 1500 K in our case), at 1 ns (corresponding to the beginning of the pulse), 6 ns (at the maximum of the pulse), 12 ns (end of the pulse), and 2.7 ms (i.e. at the end of the afterglow). The corresponding vibrational temperatures, which can be considered as a measure of the vibrational population, are also presented in figure 11 (in the same color as the curves). They are calculated by the population of CO_2(V1) and CO_2(V2)), but the dashed lines (in the same color) indicate the densities of all levels (according to the Boltzmann distributions at these temperatures).

Once the pulse power is applied, CO_2 is populated immediately into vibrational states from the ground state. During the pulse (until 12 ns), the vibrational levels are primarily populated by electron impact excitation, and at the end of the pulse, about 50 % and 30% of CO_2 is excited into the symmetric (a-d) and asymmetric (1-21) mode levels, respectively, while only 20% is in the CO_2 ground state. During the pulse, the VDF of CO_2 is far from thermal equilibrium, corresponding to a high vibrational temperature. The highest vibrational temperature of 4904 K is reached at the end of the pulse, which is almost 3 times the gas temperature. This means that the NPD plasma is clearly non-thermal. After pulse termination, the density of the high vibrational levels rapidly decreases. This is because the high vibrational levels relax significantly faster than the low vibrational levels,

as the vibration-translation (VT) and vibration-vibration (VV') relaxation rates increase for higher vibrational levels [64]. The VDF of the asymmetric mode levels becomes thermal at 2.7 ms (with a vibrational temperature of 1557 K, close to the gas temperature), while the symmetric mode levels are still significantly populated.

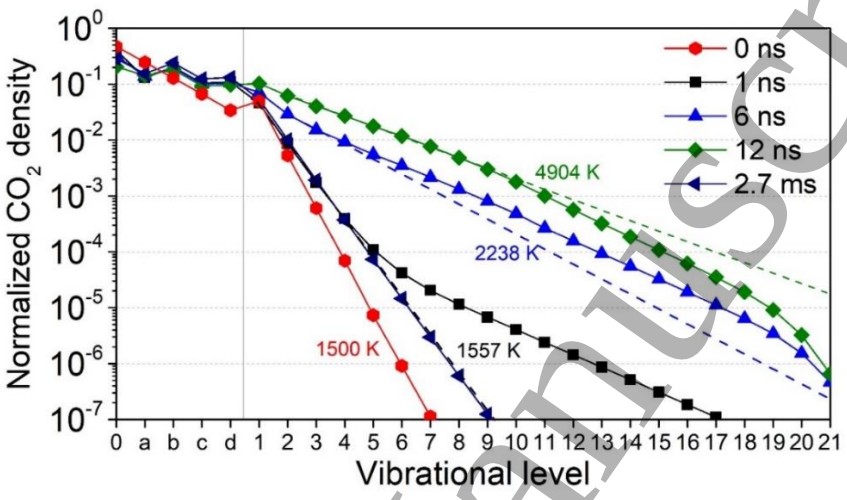

Figure 11. Vibrational distribution function (VDF) of CO_2 in the NPD at different times within one pulse (until 12 ns) and after the pulse (2.7 ms), at an SEI of 5.1 kJ/L. The notations '0', 'a-d' and '1-21' in the x-axis represent the CO_2 ground state, the effective symmetric mode levels, and the asymmetric mode vibrational levels up to the dissociation limit, respectively. Besides the calculated VDFs (solid lines), the so-called vibrational temperature is also indicated (next to the curve, in the same color); it is calculated from the population of CO_2(V1) and CO_2(V2), but the dashed lines indicate the population of the higher levels according to this temperature, following a Boltzmann distribution.

As the vibrational levels of CO_2 are quite important during the pulse, we calculated their contributions to the loss processes of CO_2; see figure 12 and table 4. Electron impact dissociation from the CO_2 vibrational levels contributes for 74%, mainly from the four effective symmetric mode levels (52%) and the lower (V1-V4) or middle asymmetric mode levels (V5-V15) (16% and 6%, respectively), while the same process from the CO_2 ground state contributes for 26%. In addition, dissociation upon reaction of CO_2 with H atoms mostly occurs from the middle vibrational levels (V5-V15) with a contribution of 92.7%. Indeed, the energy of the middle vibrational levels is comparable to or even higher than the activation energy of reaction between CO_2 and H atoms. As the activation energy of the reaction of CO_2 with any molecule M is much higher (5.6 eV), the dissociation by this reaction is almost entirely from the highest vibrational levels (V16-V21) (98.9%), while the middle vibrational levels only contribute for 1.1%, and the ground state, the four

effective symmetric mode levels and the four lower asymmetric mode levels have nearly no contribution to this dissociation process. When looking at the overall CO_2 dissociation, the vibrational levels contribute for 85%, and the symmetric mode levels, low, middle and highest asymmetric mode levels all seem important (see figure 11 and table 6), while the ground state only contributes for 15%. Thus, vibrational excitation plays a crucial role for CO_2 dissociation in DRM by NPD.

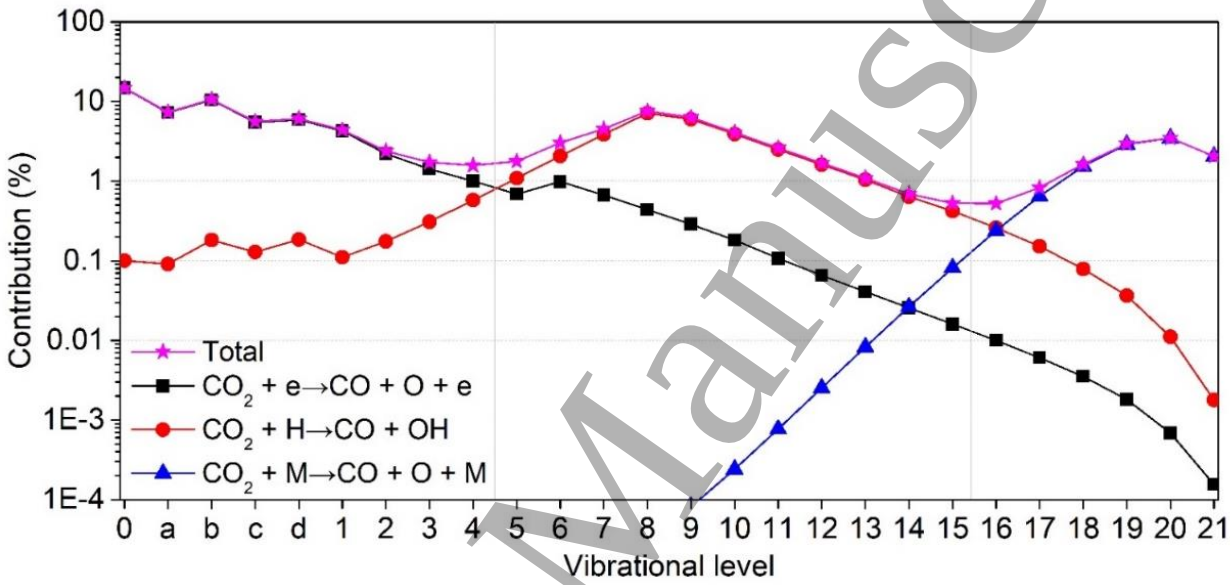

Figure 12. Contribution of the CO_2 ground state and the various vibrational levels to the total dissociation of CO_2, at an SEI of 5.1 kJ/L. Note that in this case only the dissociation reactions are accounted for, and not the reverse reactions.

Table 5: Contribution of the CO_2 ground state, symmetric mode levels (Va-Vd), lower (V1-V4), middle (V5-V15), and higher (V16-V21) asymmetric mode vibrational levels to the total CO_2 dissociation, and to the different mechanisms

	Ground state	**Va-Vd**	**V1-V4**	**V5-V15**	**V16-V21**
Total dissociation	15%	30%	10%	34%	11%
$CO_2 + e \rightarrow CO + O + e$	26%	52%	16%	6%	0%
$CO_2 + H \rightarrow CO + OH$	0.3%	1.8%	3.6%	92.7%	1.6%
$CO_2 + M \rightarrow CO + O + M$	0%	0%	0%	1.1%	98.9%

When looking at the individual mechanisms important for the CO_2 ground state and the various vibrational levels (shown in table 6), we see that dissociation from the ground state proceeds mainly by electron impact (99%). Note that this is electron impact dissociation

by excitation to a repulsive excited state (so-called excitation-dissociation). For the low vibrational levels, i.e., the symmetric mode levels (Va -Vd) and the lower asymmetric mode levels (V1-V4), most of the dissociation (98% and 88%, respectively) also occurs from electron impact excitation-dissociation. On the other hand, the collision with H atoms is the most important dissociation reaction from the middle levels (V5-V15), with a contribution of 89%, while electron impact dissociation only contributes for about 10%. For the highest vibrational level (V16-V21), dissociation upon reaction with any molecule M become most important (95%), while the reaction with H atoms and electron impact excitation-dissociation only contribute for 4.7% and 0.2%, respectively.

Table 6: Contribution of the individual dissociation mechanisms for the CO_2 ground state, symmetric mode levels (Va-Vd), lower (V1-V4), middle (V5-V15), and higher (V16-V21) asymmetric mode vibrational levels

	Ground state	Va-Vd	V1-V4	V5-V15	V16-V21
$CO_2 + e \rightarrow CO + O + e$	99.3%	98%	88.4%	10.3%	0.2%
$CO_2 + H \rightarrow CO + OH$	0.7%	2%	11.6%	89.3%	4.7%
$CO_2 + M \rightarrow CO + O + M$	0%	0%	0%	0.4%	95.1%

The important role of the vibrationally excited levels in CO_2 dissociation is also found in GA and MW plasmas. However, due to the high gas temperature of GA plasmas (above 3000 K), the VDF of CO_2 is quasi-Boltzmann, so that most CO_2 dissociation occurs from the symmetric-mode vibrational levels (Va -Vd), which have the lowest energy [42]. Similarly, 0D modeling of CO_2 splitting in Ref. [64] indicated that the vibrational levels with energies above 1 eV play a negligible role in MW plasma with a gas temperature of 1000 and 2000 K. The differences in the contributions of the vibrational levels with our study are mainly because the vibrational levels of CO_2 are highly overpopulated in the NPD, thus playing a more prominent role in the CO_2 conversion.

Comparing our results for DRM (at an SEI of 5.1 kJ/L, i.e., 1.3 eV per molecule) with those for pure CO_2 splitting (at an SEI of 1.6 eV per molecule) in the NPD [54], we can conclude that the important loss process of CO_2 in both cases are electron impact dissociation, and in both cases all the symmetric and asymmetric mode levels are important. The second important CO_2 loss process in case of DRM is the reaction of CO_2 with H atoms

(see figure 6(a, c)), which are formed directly from the dissociation of CH_4, so they have a much higher density than the O atoms, see figure 5(c). As the threshold energy of the reaction between CO_2 and H atoms is lower than that of the reaction of CO_2 and O atoms, the middle vibrational levels have a higher contribution for the CO_2 conversion in case of DRM than in pure CO_2 splitting in the NPD. Because the SEI in our case is somewhat lower than in Ref. [54], the contribution of the highest vibrational levels is somewhat lower, and vice versa, the contribution of the ground state is a little bit higher.

4. Conclusion

We developed a chemical kinetics model to investigate the underlying plasma chemistry of dry reforming of methane (DRM) in a NPD. The calculated CO_2 and CH_4 conversions and the selectivities of the main products were compared with experimental results in a wide range of SEI values, and good agreement was reached, indicating that our model is able to provide a realistic picture of the plasma chemistry of DRM in a NPD.

The densities of the main products (i.e., CO, H_2, and light hydrocarbons) and of the most important radicals and ions, as well as the electrons, are presented as a function of time during the ns-pulse and its afterglow. In addition, the dominant loss and formation processes of CO_2 and CH_4, as well as the most important formation reactions of the major products, i.e., CO, H_2, C_2H_2, C_2H_4, C_2H_6 and C_3H_6, are explored. Our model reveals that the most important dissociation reactions of CO_2 and CH_4 are electron impact dissociation of CO_2 into CO and O, and dissociation of CH_4 into CH_3 and H. Likewise, the dominant formation reaction of CO is electron impact dissociation of CO_2, but dissociation of CO_2 upon collision with H radicals is also quite important. The most important production process of H_2 is the reaction of CH_4 with H radicals. C_2H_2 is the most abundant hydrocarbon product at longer time-scales, and its most important formation reaction is the recombination of two CH_2 radicals. The CH_3 radicals are also important intermediate radicals, and they play a crucial role in the formation of the various hydrocarbon products. Indeed, the recombination of CH_3 with C_2H_5 is the most important formation reaction of C_2H_4, while the most important formation reactions of C_2H_6 and C_3H_8 are the three-body recombination of two CH_3 radicals, and the three-body recombination of CH_3 with C_2H_5 radicals, respectively.

Finally, our model reveals that the vibrationally excited levels of CO_2 play an important role in CO_2 dissociation in case of DRM by NPD. When looking at the overall CO_2 dissociation, the ground state only contributes for 15%, while the vibrational levels contribute for 85%. For the low vibrational levels (Va-Vd, V1-V4), most of the dissociation occurs by electron impact reactions, while the collision with H atoms is the most important dissociation reaction for the middle vibrational levels (V5-V16), and dissociation of CO_2 upon collision with any molecule M becomes the most important for the highest vibrational levels (V17-V21).

We believe that our chemical kinetics model provides a better insight in the main chemistry mechanisms of DRM in NPD. Compared with other plasma types, DRM by NPD is quite promising. However, we believe there is still room for improvement. Our modeling results show that the most important loss processes of CO_2 and CH_4 are electron impact dissociation, which suggests that we can improve the performance by increasing the electron number density, for example, by pre-ionization of the gases using a laser to increase the density of seed electrons, although this would also increase the energy cost, or by reducing the interpulse time (using a burst mode), due to a memory effect from the previous pulse, as observed in recent experiments [56,57]. Furthermore, the simulation shows that the selectivity of the light hydrocarbon products is determined by the dehydrogenation degree of CH_4, indicating that we can regulate the product selectivity by tuning the electron temperature, i.e., tuning the reduced electric field (by optimizing the discharge electrical operating parameters or electrode design).

5. Acknowledgements

This work is supported by the National Natural Science Foundation of China (Grant No. 52077026, 11965018), L Zhang was also supported by the China Scholarship Council (CSC).

6. References

[1] Anon 2018 NASA: Global climate changes, climate change: Evidence.

[2] Scapinello M, Delikonstantis E and Stefanidis G D 2017 The panorama of plasma-assisted non-oxidative methane reforming *Chem. Eng. Process. Process Intensif.* **117** 120–40

[3] Tu X, Gallon H J, Twigg M V, Gorry P A and Whitehead J C 2011 Dry reforming of methane over a Ni/Al_2O_3 catalyst in a coaxial dielectric barrier discharge reactor *J. Phys. D. Appl. Phys.* **44** 274007

[4] Zhou L M, Xue B, Kogelschatz U and Eliasson B 1998 Nonequilibrium plasma reforming of greenhouse gases to synthesis gas *Energy & Fuels* **12** 1191–9

[5] Karakaya C and Kee R J 2016 Progress in the direct catalytic conversion of methane to fuels and chemicals *Prog. Energy Combust. Sci.* **55** 60–97

[6] Snoeckx R and Bogaerts A 2017 Plasma technology – a novel solution for CO_2 conversion? *Chem. Soc. Rev.* **46** 5805–63

[7] Tu X and Whitehead J C 2012 Plasma-catalytic dry reforming of methane in an atmospheric dielectric barrier discharge: Understanding the synergistic effect at low temperature *Appl. Catal. B Environ.* **125** 439–48

[8] Zhang X and Cha M S 2013 Electron-induced dry reforming of methane in a temperature-controlled dielectric barrier discharge reactor *J. Phys. D. Appl. Phys.* **46** 415205

[9] Ozkan A, Dufour T, Arnoult G, Keyzer P De, Bogaerts A and Reniers F 2015 CO_2–CH_4 conversion and syngas formation at atmospheric pressure using a multi-electrode dielectric barrier discharge *J. CO_2 Util.* **9** 74–81

[10] Martini L M, Dilecce G, Guella G, Maranzana A, Tonachini G and Tosi P 2014 Oxidation of CH_4 by CO_2 in a dielectric barrier discharge *Chem. Phys. Lett.* **593** 55–60

[11] Yao S L, Okumoto M, Nakayama A and Suzuki E 2001 Plasma reforming and coupling of methane with carbon dioxide *Energy & Fuels* **15** 1295–9

[12] Aziznia A, Bozorgzadeh H R, Seyed-Matin N, Baghalha M and Mohamadalizadeh A 2012 Comparison of dry reforming of methane in low temperature hybrid plasma-catalytic corona with thermal catalytic reactor over $Ni/\gamma\text{-}Al_2O_3$ *J. Nat. Gas Chem.* **21** 466–75

[13] Zhu B, Li X-S, Liu J-L and Zhu A-M 2012 Optimized mixed reforming of biogas with O_2 addition in spark-discharge plasma *Int. J. Hydrogen Energy* **37** 16916–24

[14] Zhu B, Li X-S, Liu J-L, Zhu X and Zhu A-M 2015 Kinetics study on carbon dioxide reforming of methane in kilohertz spark-discharge plasma *Chem. Eng. J.* **264** 445–52

[15] Shapoval V, Marotta E, Ceretta C, Konjevič N, Ivkovič M, Schiorlin M and Paradisi C 2014 Development and testing of a self-triggered spark reactor for plasma driven dry reforming of methane *Plasma Process. Polym.* **11** 787–97

[16] Shapoval V and Marotta E 2015 Investigation on plasma-driven methane dry reforming in a self-triggered spark reactor *Plasma Process. Polym.* **12** 808–16

[17] Tu X and Whitehead J C 2014 Plasma dry reforming of methane in an atmospheric pressure AC gliding arc discharge: Co-generation of syngas and carbon nanomaterials *Int. J. Hydrogen Energy* **39** 9658–69

[18] Cleiren E, Heijkers S, Ramakers M and Bogaerts A 2017 Dry reforming of methane in a gliding arc plasmatron: Towards a better understanding of the plasma chemistry *ChemSusChem* **10** 4025–36

[19] Slaets J, Aghaei M, Ceulemans S, Van Alphen S and Bogaerts A 2020 CO_2 and CH_4 conversion in "real" gas mixtures in a gliding arc plasmatron: How do N_2 and O_2 affect the performance? *Green Chem.* **22** 1366–77

[20] Van Alphen S, Slaets J, Ceulemans S, Aghaei M, Snyders R and Bogaerts A 2021 Effect of N_2 on CO_2-CH_4 conversion in a gliding arc plasmatron: Can this major component in industrial emissions improve the energy efficiency? *J. CO_2 Util.* **54** 101767

[21] Fidalgo B, Domínguez A, Pis J J and Menéndez J A 2008 Microwave-assisted dry reforming of methane *Int. J. Hydrogen Energy* **33** 4337–44

[22] Chun S M, Hong Y C and Choi D H 2017 Reforming of methane to syngas in a microwave plasma torch at atmospheric pressure *J. CO_2 Util.* **19** 221–9

[23] Li D, Li X, Bai M, Tao X, Shang S, Dai X and Yin Y 2009 CO_2 reforming of CH_4 by atmospheric pressure glow discharge plasma: A high conversion ability *Int. J. Hydrogen Energy* **34** 308–13

[24] Wanten B, Maerivoet S, Vantomme C, Slaets J, Trenchev G and Bogaerts A 2022 Dry reforming of methane in an atmospheric pressure glow discharge: Confining the plasma to expand the performance *J. CO_2 Util.* **56** 101869

[25] Scapinello M, Martini L M, Dilecce G and Tosi P 2016 Conversion of CH_4/CO_2 by a nanosecond repetitively pulsed discharge *J. Phys. D. Appl. Phys.* **49** 75602

[26] Kosarev I N, Khorunzhenko V I, Mintoussov E I, Sagulenko P N, Popov N A and Starikovskaia S M 2012 A nanosecond surface dielectric barrier discharge at elevated pressures: time-resolved electric field and efficiency of initiation of combustion *Plasma Sources Sci. Technol.* **21** 45012

[27] Zhang L, Yang D, Wang W, Wang S, Yuan H, Zhao Z, Sang C and Jia L 2016 Needle-array to plate DBD plasma using sine AC and nanosecond pulse excitations for purpose of improving indoor air quality *Sci. Rep.* **6** 25242

[28] Snoeckx R, Zeng Y X, Tu X and Bogaerts A 2015 Plasma-based dry reforming: improving the conversion and energy efficiency in a dielectric barrier discharge *RSC Adv.* **5** 29799–808

[29] Snoeckx R, Aerts R, Tu X and Bogaerts A 2013 Plasma-based dry reforming: A computational study ranging from the nanoseconds to seconds time scale *J. Phys. Chem. C* **117** 4957–70

[30] Bie C De, van Dijk J and Bogaerts A 2015 The dominant pathways for the conversion of methane into oxygenates and syngas in an atmospheric pressure dielectric barrier discharge *J. Phys. Chem. C* **119** 22331–50

[31] Pancheshnyi S. E B H G J M P L C Computer code ZDPlasKin, http://www.zdplaskin.laplace.univ-tlse.fr, (University of Toulouse, LAPLACE, CNRS-UPS-INP, Toulouse, France,2008)

[32] Wang W, Snoeckx R, Zhang X, Cha M S and Bogaerts A 2018 Modeling plasma-based CO_2 and CH_4 conversion in mixtures with N_2, O_2, and H_2O: The bigger plasma chemistry picture *J. Phys. Chem. C* **122** 8704–23

[33] Heijkers S 2020 *Plasma chemistry modelling for CO_2 and CH_4 conversion in various plasma types* (PhD thesis, University of Antwerp)

[34] Yoon J-S, Song M-Y, Han J-M, Hwang S H, Chang W-S, Lee B and Itikawa Y 2008 Cross sections for electron collisions with hydrogen molecules *J. Phys. Chem. Ref. Data* **37** 913–31

[35] Woodall J, Agúndez M, Markwick-Kemper A J and Millar T J 2007 The UMIST database for astrochemistry 2006 *A&A* **466** 1197–204

[36] Anon Morgan Database www.lxcat.net. (retrieved 1 July 2017)

[37] Tian C and Vidal C R 1998 Cross sections of the electron impact dissociative ionization of CO, and *J. Phys. B At. Mol. Opt. Phys.* **31** 895–909

[38] Itikawa Y 2002 Cross sections for electron collisions with carbon dioxide *J. Phys. Chem. Ref. Data* **31** 749–67

[39] Hake R D and Phelps A V 1967 Momentum-transfer and inelastic-collision cross sections for electrons in O_2, CO, and CO_2 *Phys. Rev.* **158** 70–84

[40] Lowke J J, Phelps A V. and Irwin B W 2003 Predicted electron transport coefficients and operating characteristics of CO_2–N_2–He laser mixtures *J. Appl. Phys.* **44** 4664

[41] Anon Phelps, A. V. Phelps Database www.lxcat.net.

[42] Nikitin A V, Rey M and Tyuterev V G 2011 Rotational and vibrational energy levels of methane calculated from a new potential energy surface *Chem. Phys. Lett.* **501** 179–86

[43] Song M-Y, Yoon J-S, Cho H, Itikawa Y, Karwasz G P, Kokoouline V, Nakamura Y and Tennyson J 2015 Cross sections for electron collisions with methane *J. Phys. Chem. Ref. Data* **44** 23101

[44] Itikawa Y and Mason N 2005 Cross sections for electron collisions with water molecules *J. Phys. Chem. Ref. Data* **34** 1–22

[45] Trajmar S, Register D F and Chutjian A 1983 Electron scattering by molecules II. Experimental methods and data *Phys. Rep.* **97** 219–356

[46] Janev R K and Reiter D 2004 Collision processes of $C_{2,3}H_y$ and $C_{2,3}H_y^+$ hydrocarbons with electrons and protons *Phys. Plasmas* **11** 780–829

[47] Janev R K and Reiter D 2003 Collision processes of hydrocarbon species in hydrogen plasmas. Part 2. The ethane and propane families *ChemInform* **34**

[48] Janev R K and Reiter D 2002 Collision processes of CH_y and CH_y^+ hydrocarbons with plasma electrons and protons *Phys. Plasmas* **9** 4071–81

[49] K J R 1995 *Atomic and Molecular Processes in Fusion Edge Plasmas* (New York, U.S.A: Plenum Press)

[50] Zhu B, Li X, Shi C, Liu J, Zhao T and Zhu A 2012 Pressurization effect on dry reforming of biogas in kilohertz spark-discharge plasma *Int. J. Hydrogen Energy* **37** 4945–54

[51] Castela M, Stepanyan S, Fiorina B, Coussement A, Gicquel O, Darabiha N and Laux C O 2017 A 3-D DNS and experimental study of the effect of the recirculating flow pattern inside a reactive kernel produced by nanosecond plasma discharges in a methane-air mixture *Proc. Combust. Inst.* **36** 4095–103

[52] Delikonstantis E, Scapinello M, Van Geenhoven O and Stefanidis G D 2020 Nanosecond pulsed discharge-driven non-oxidative methane coupling in a plate-to-plate electrode configuration plasma reactor *Chem. Eng. J.* **380** 122477

[53] Stepanyan S, Minesi N, Tibère-Inglesse A, Salmon A, Stancu G D and Laux C O 2019 Spatial evolution of the plasma kernel produced by nanosecond discharges in air *J. Phys. D. Appl. Phys.* **52** 295203

[54] Heijkers S, Martini L M, Dilecce G, Tosi P and Bogaerts A 2019 Nanosecond pulsed discharge for CO_2 Conversion: Kinetic modeling to elucidate the chemistry and improve the performance *J. Phys. Chem. C* **123** 12104–16

[55] Zhao Z and Li J 2020 Repetitively pulsed gas discharges: memory effect and discharge mode transition *High Volt.* **5** 569–82

[56] Montesano C, Faedda M, Martini L M, Dilecce G and Tosi P 2021 CH_4 reforming with CO_2 in a nanosecond pulsed discharge. The importance of the pulse sequence *J. CO_2 Util.* **49** 101556

[57] Montesano C, Quercetti S, Martini L M, Dilecce G and Tosi P 2020 The effect of different pulse patterns on the plasma reduction of CO_2 for a nanosecond discharge *J. CO_2 Util.* **39** 101157

[58] Lotfalipour R, Ghorbanzadeh A M and Mahdian A 2014 Methane conversion by repetitive nanosecond pulsed plasma *J. Phys. D. Appl. Phys.* **47** 365201

[59] Aerts R, Martens T and Bogaerts A 2012 Influence of vibrational states on CO_2 splitting by dielectric barrier discharges *J. Phys. Chem. C* **116** 23257–73

[60] Van Alphen S, Vermeiren V, Butterworth T, Van Den Bekerom D C M, Van Rooij G J and Bogaerts A 2020 Power pulsing to maximize vibrational excitation efficiency in N_2 microwave plasma: a combined experimental and computational study *J. Phys. Chem. C* **124** 1765–79

[61] Lašič Jurković D, Liu J-L, Pohar A and Likozar B 2021 Methane dry reforming over Ni/Al_2O_3 catalyst in spark plasma reactor: Linking computational fluid dynamics (CFD) with reaction kinetic modelling *Catal. Today* **362** 11–21

[62] Bouwman D, Martinez A, Braams B J and Ebert U 2021 Neutral dissociation of methane by electron impact and a complete and consistent cross section set *Plasma Sources Sci. Technol.* **30** 75012

[63] Bogaerts A, Berthelot A, Heijkers S, Kolev S, Snoeckx R, Sun S, Trenchev G, Laer K Van and Wang W 2017 CO_2 conversion by plasma technology: Insights from modeling the plasma chemistry and plasma reactor design *Plasma Sources Sci. Technol.* **26** 063001

[64] Kozák T and Bogaerts A 2014 Splitting of CO_2 by vibrational excitation in non-equilibrium plasmas: a reaction kinetics model *Plasma Sources Sci. Technol.* **23** 45004

[65] Kozák T and Bogaerts A 2015 Evaluation of the energy efficiency of CO_2 conversion in microwave discharges using a reaction kinetics model *Plasma Sources Sci. Technol.* **24** 15024–40

[66] Berthelot A and Bogaerts A 2017 Modeling of CO_2 splitting in a microwave plasma: How to improve the conversion and energy efficiency *J. Phys. Chem. C* **121** 8236–51

[67] Wang W, Mei D, Tu X and Bogaerts A 2017 Gliding arc plasma for CO_2 conversion: Better insights by a combined experimental and modelling approach *Chem. Eng. J.* **330** 11–25

[68] Silva T, Britun N, Godfroid T and Snyders R 2014 Optical characterization of a microwave pulsed discharge used for dissociation of CO_2 *Plasma Sources Sci. Technol.* **23** 025009

[69] Sun S R, Wang H X, Mei D H, Tu X and Bogaerts A 2017 CO_2 conversion in a gliding arc plasma: Performance improvement based on chemical reaction modeling *J. CO_2 Util.* **17** 220–34

[70] Heijkers S and Bogaerts A 2017 CO_2 conversion in a gliding arc plasmatron: elucidating the chemistry through kinetic modeling *J. Phys. Chem. C* **121** 22644–55

[71] Berthelot A and Bogaerts A 2018 Pinpointing energy losses in CO_2 plasmas – Effect on CO_2 conversion *J. CO_2 Util.* **24** 479–99

[72] Pietanza L D, Colonna G, D'Ammando G, Laricchiuta A and Capitelli M 2015 Vibrational excitation and dissociation mechanisms of CO_2 under non-equilibrium discharge and post-discharge conditions *Plasma Sources Sci. Technol.* **24** 042002